Group Analysis of DTI Fiber Tract Statistics with Application to Neurodevelopment

Casey B. Goodlett [a,*] P. Thomas Fletcher [a] John H. Gilmore [b]
Guido Gerig [a]

[a] *University of Utah, Salt Lake City, Utah, United States*

[b] *University of North Carolina, Chapel Hill, North Carolina, United States*

Abstract

Diffusion tensor imaging (DTI) provides a unique source of information about the underlying tissue structure of brain white matter *in vivo*, including both the geometry of major fiber bundles as well as quantitative information about tissue properties as represented by measures such as tensor orientation, anisotropy, and size. This paper presents a method for statistical comparison of fiber bundle diffusion properties between populations of diffusion tensor images. Unbiased diffeomorphic atlas building is used to compute a normalized coordinate system for populations of diffusion images. The smooth invertible nature of the transformations between each subject and the atlas provides spatial normalization for the comparison of tract statistics. Diffusion properties, such as fractional anisotropy (FA) and tensor size, of fiber tracts are modeled as multivariate functions of arc length. Hypothesis testing of tract models is performed non-parametrically with permutation testing based on the Hotelling T^2 statistic. The linear discriminant embedded in the T^2 metric provides an intuitive, localized interpretation of detected differences. The proposed methodology was tested on a clinical study of neurodevelopment. In a study of one

and two year old subjects, a significant increase in FA and a correlated decrease in Frobenius norm was found in several tracts. Significant differences in neonates were found in the splenium tract between controls and subjects with isolated mild ventriculomegaly (MVM) demonstrating the potential of this method for clinical studies.

Key words: Diffusion tensor imaging; Registration; Tract modeling; Neurodevelopment; Statistical Modeling

1 Introduction

Clinical neuroimaging studies increasingly rely on diffusion tensor imaging (DTI) for new insights into the tissue structure of brain white matter *in vivo*. Traditional structural magnetic resonance imaging (MRI) provides little contrast withing the white matter, which is displayed as a homogeneous volume without information about the underlying tissue orientation and microstructure. DTI, on the other hand, provides information about the axon bundles of the white matter such as preferred orientation, myelination, and density as reflected in measures of the diffusion tensor for each voxel (Basser and Pierpaoli, 1996). The diffusion tensor incorporates information about the preferred fiber orientation in the principal eigenvector as well as information about local tissue structure in measures of anisotropy and tensor size. This paper addresses the problem of normalizing geometric models of white matter bundles and making statistical inference about differences in diffusion properties.

* Corresponding author.
Email address: gcasey@sci.utah.edu (Casey B. Goodlett).

Most approaches to group analysis in the clinical DTI literature have relied on voxel based morphometry (VBM) or manually drawn regions of interest. An overview of the differences between VBM and ROI analysis in DTI population studies was described by Snook et al. (2007). Voxel based analysis methods are characterized by alignment of images to a template followed by independent hypothesis tests per voxel which are smoothed and corrected for multiple comparisons. Voxelwise analysis has been applied in DTI studies of autism (Barnea-Goraly et al., 2004), schizophrenia (Burns et al., 2003), and Alzheimer's disease (Sydykova et al., 2007). The major challenge in VBM analysis is the need for complex multiple comparison correction and the need for smoothing methods which can make localization of changes challenging to interpret (Jones et al., 2005a). Other studies have used manually drawn regions of interest (ROIs) for group comparison of DTI properties. Within the ROIs, diffusion properties such as FA or mean diffusivity (MD) are averaged to create a single statistic. Examples of studies using ROI methods can be found in normal development (Bonekamp et al., 2007; Gilmore et al., 2007a; Hermoye et al., 2006), schizophrenia (Kubicki et al., 2005), and Krabbe disease (Guo et al., 2001). The major drawback of ROI analysis is the time consuming nature of manual identification of regions, especially the ability to identify the long curved structures common in DTI fiber tracts. Our method improves on previous methods in the ability to perform automatic processing through the use of high dimensional registration as well as the ability to focus on testing specific hypotheses regarding tracts of interest using a novel method for joint analysis of tensor shape measures in a tract model.

Segmenting anatomically known fiber bundles remains an important challenge for DTI analysis. The most common approach, fiber tractography, integrates

the field of tensor principal eigenvector to create streamlines which sample anatomical fiber bundles (Basser et al., 2000). Corouge et al. (2006), Jones et al. (2005b), and Lin et al. (2006) proposed to analyze the diffusion properties of fiber tracts as a function of arc length. More recent work has focused on volumetric segmentation methods which also allow data within the tract to be reduced to a function of arc length (Fletcher et al., 2007; Melonakos et al., 2007). These methods emphasize the need to understand diffusion properties in the context of geometric models of fiber bundles.

The major challenge in implementing tract oriented statistics in population studies is finding a consistent spatial parametrization within and between populations. Defining anatomically equivalent ROIs to seed tractography for large population studies is time consuming, error prone, and often requires significant post-processing such as cleaning and clustering. Furthermore, even given tractography seeds for each image, the natural variability of brain size and shape prohibits an automatic consistent parametrization for arc length models of diffusion. To solve both the needs for tract segmentation in individual cases as well as shape normalization for fiber tracts, we apply a population based registration method. Jones et al. (2002) and Xu et al. (2003) initially described the advantages of spatial normalization for DTI population studies. Recent work has focused on the use of unbiased methods for mapping tensor images to a common coordinate system (Zhang et al., 2007; Peyrat et al., 2007). A reference atlas of fiber bundles visible in DTI was produced by Mori et al. (2005). Xu et al. (2008) highlighted the need for smooth invertible mappings in a registration framework. Other work on DTI atlas building has used the geometry information contained within tractography results rather than image registration to build a population model (O'Donnell and Westin, 2007).

In our framework, atlas building for DTI creates a global spatial normalization which can be used to parametrize tract oriented measures across a population.

In work closely related to the proposed methodology, Yushkevich et al. (2008) propose a method for statistical analysis along the two-dimensional medial manifolds of fiber tracts for specific tracts of interest after unbiased group alignment. On the tract medial axis, permutation tests are applied to detect clusters of pointwise differences between MD of groups. Another approach proposed by Smith et al. (2006), tract-based spatial statistics, is a global approach for analysis of diffusion properties using non-linear registration to a template combined with a skeletonization of FA voxels. FA values are globally projected onto the skeleton followed by pointwise hypothesis tests on the skeleton. Our method differs from these primarily in the use of statistical analysis that incorporate multivariate tensor measure and tract-oriented statistics for a single hypothesis test per-tract.

This paper present a method for group comparison of DTI that combines a method for high-dimensional diffeomorphic registration with a statistical framework for detecting and understanding differences between the diffusion properties of fiber tracts. The emphasis of the DTI atlas building procedure is to model and normalize the geometry of fiber bundles to analyze differences of diffusion properties between groups. A schematic overview of the procedure is shown in Fig. 1. Atlas building is performed based on a feature which is sensitive to the medial location of brain white matter. The diffusion properties of fiber bundles are modeled as continuous spatial functions of arc length, where the tract functions are multivariate functions which map arc length to orthogonal measures of tensor shape. Statistics appropriate to populations of continuous functions is applied for hypothesis testing and discrimination. The

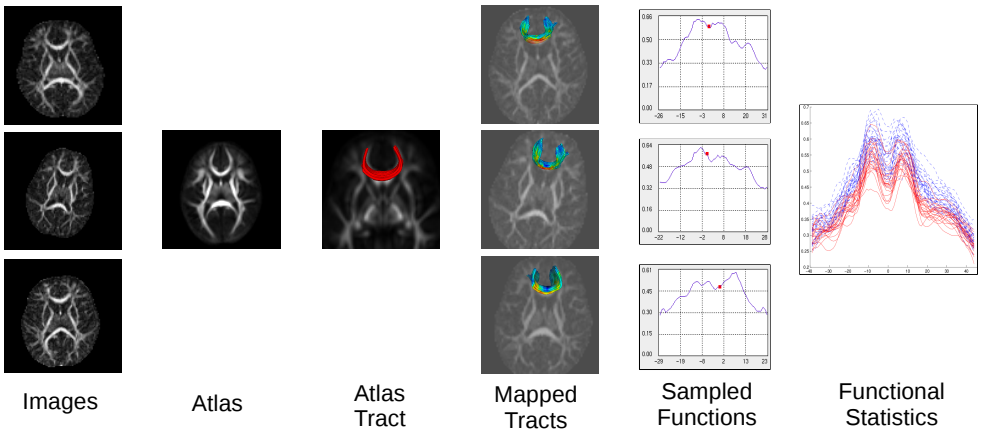

Fig. 1. Schematic overview of the tract analysis procedure. A population of images is first mapped into an atlas which is used to generate a template fiber tract. Inverse transformations are used to map the template tract back into the individual subjects to collect along tract measurements of tensor properties. The parametrization given by the atlas is used to compute statistics on the spatial functions.

key contributions of this paper are the use of atlas building to parametrize fiber tract statistics and a method for statical inference in populations of tract oriented diffusion statistics. The proposed methodology was evaluated on a large pediatric study of normal development and comparison in neonates of controls to MVMs who are at higher risk for mental illness.

2 DTI Atlas Building

Comparison of diffusion properties in populations of diffusion tensor images requires a method for identifying corresponding regions of anatomy. We have extended a high-dimensional, unbiased registration procedure developed by Joshi et al. (2004) using a feature image that is sensitive to the geometry of brain white matter and is similar in spirit to methods proposed in the literature for modeling white matter by its medial sheet (Smith et al., 2006; Kindlmann

et al., 2007). The goal of the atlas building procedure is to provide spatial normalization for analysis of diffusion values at corresponding locations. Further reference on the DTI atlas building procedure is described by Goodlett et al. (2006).

Diffusion tensors are estimated for each subject from the diffusion weighted images using weighted least squares tensor estimation (Salvador et al., 2005). The atlas building procedure is initialized by affine registration of the baseline image of each subject to a T2 weighted atlas using normalized mutual information. Skull stripping is performed by applying a segmentation tool on the baseline image to create a mask of non-brain regions. After affine alignment and skull stripping, a feature image is computed for each subject. Given a tensor image I and the corresponding FA image FA, the feature image C is defined as the maximum absolute eigenvalue of the Hessian of the FA image. The Hessian is computed by convolution of the FA image with a set of Gaussian second derivatives with a fixed aperture. The σ value for the kernel is chosen empirically to be proportional to the size of white matter structures in the brain. For example, a smaller value is used for neonates than for adults. Figure 2 shows the FA image of a tensor field and the corresponding structural image C. We apply the atlas building procedure of Joshi et al. (2004) to the set of feature images using the parameters of the affine registration as an initialization. The result of the atlas building procedure is a set of invertible transformations which map each subject tensor image to an atlas coordinate system.

We choose the feature image C over alternative image match metrics for two main reasons. First, we observe that C is a good detector of major fiber bundles which occur as tubular or sheet-like structures. Callosal fibers form a thin

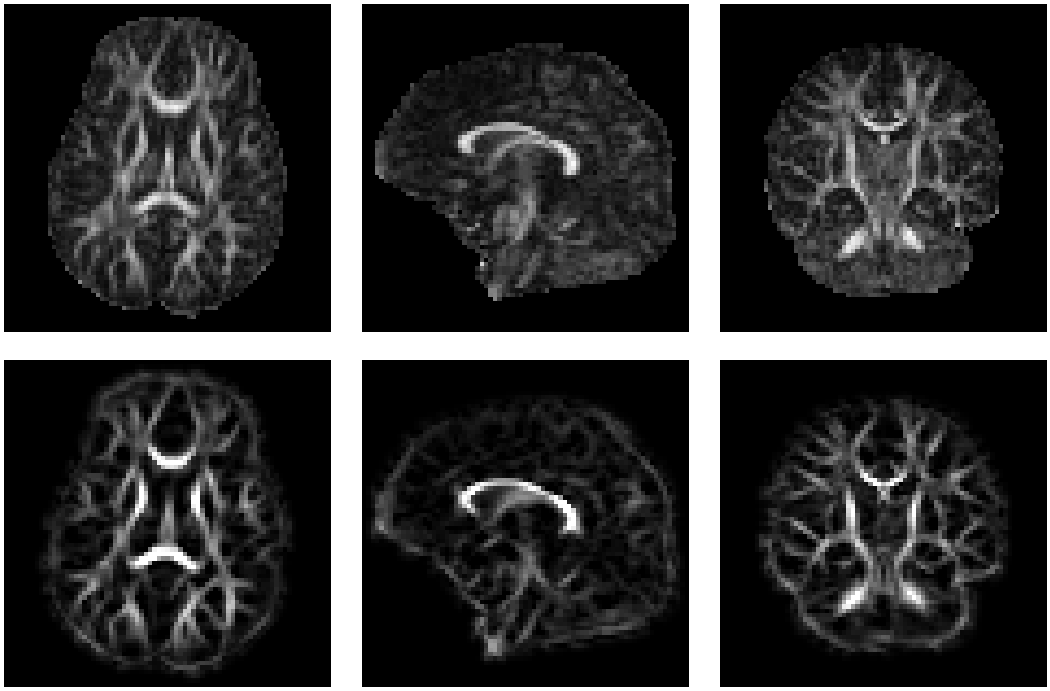

Fig. 2. The top row shows axial, sagittal, and coronal slices of the FA image from a DTI scan of a 1 year old subject. The bottom row shows the result of the structural operator on the FA image taken at $\sigma = 2.0mm$. Major fiber bundles such as the corpus callosum, fornix, and corona radiata are highlighted, while the background noise is muted.

swept U; the corona radiate is a thin fan; the cingulum is a tubular bundle, and C serves as a strong feature detector for all types of these thin structures. Consequently, C optimizes correspondence of fiber tracts better than the baseline image, because C has the strongest response at the center of major fiber bundles, while the baseline image has the strongest signal in the cerebro-spinal fluid (CSF). Secondly, we use C instead of a full tensor metric or FA itself in order to minimize overfitting the diffeomorphic registration by using the same feature for registration that will be used for statistical comparison.

After nonlinear transformations have been computed for each feature image, they are applied to the corresponding tensor images. Methods appropriate for

tensor processing are used to resample the tensor fields in the atlas space. Tensors are reoriented using the finite strain approximation proposed by Alexander et al. (2001). Given the results of Peyrat et al. (2007), we have chosen to use the finite strain over the preservation of principal diffusion direction model as we are not modeling mechanical transformations of the anatomy. During resampling, tensors are interpolated using Riemannian methods first proposed by Pennec et al. (2006) and Fletcher and Joshi (2007). For efficiency we employ the Log–Euclidean approximation of the Riemannian metric on the space of diffusion tensors (Arsigny et al., 2006). After all images are transformed into the atlas space, the transformed images are averaged using the Log-Euclidean method to produce a tensor atlas. The result of the atlas building procedure, as illustrated in Fig. 3, is a tensor image which represents the population mean and a set of smooth, invertible transformations between the atlas space and each subject image.

The tensor atlas provides an image with improved signal-to-noise ratio (SNR) that is used to create template fiber tracts. The diffusion tensors obtained from averaging across the population can be integrated in streamline tractography approaches with significantly less outliers than in noisy individual images. After creation of the template fiber diffusion, tensor statistics from the individual cases are mapped into the atlas providing a consistent parametrization of fiber tract statistics. For each subject in the population, a fiber bundle is created using the geometry of the template atlas tract but replacing the diffusion properties with those mapped from the subject. These tracts with corresponding geometry but varying diffusion properties are then compared in a novel statistical framework.

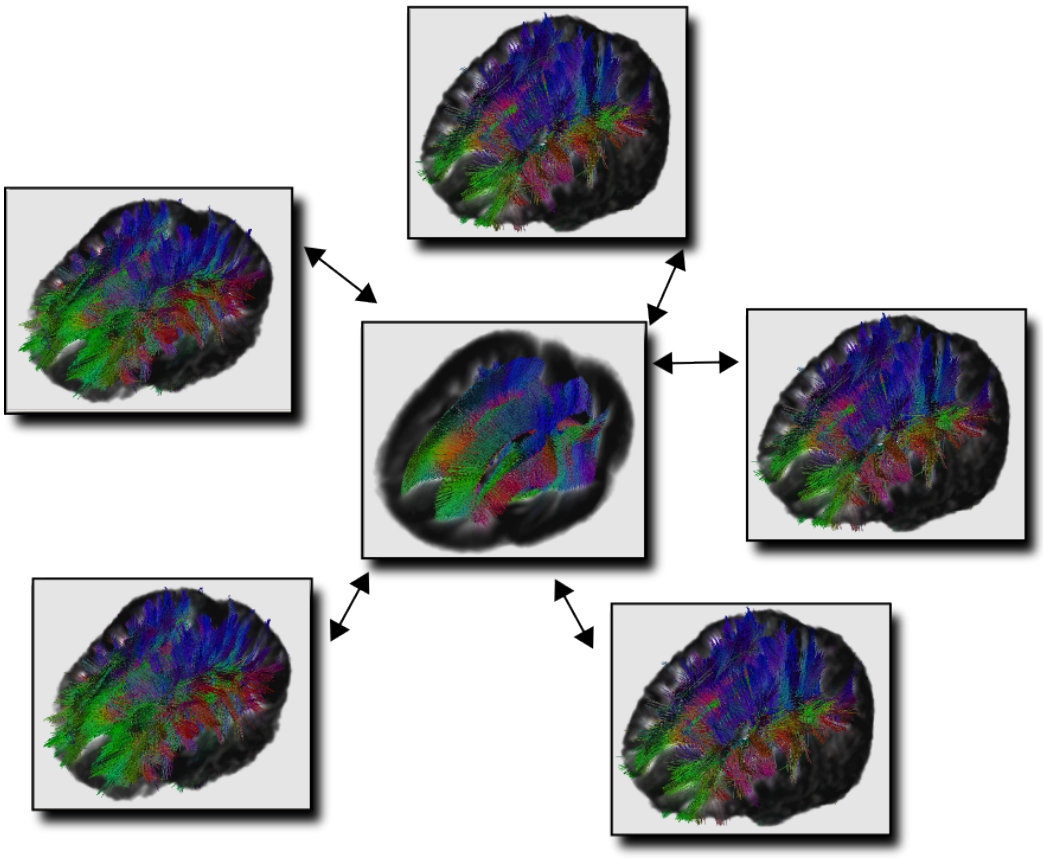

Fig. 3. Data from each subject is mapped into the atlas space using a diffeomorphic transformation. Image resampling techniques appropriate for tensor images allow the full diffusion information to be transformed.

3 Functional Analysis of Tract Properties

After spatial normalization of tensor images, corresponding values of diffusion properties within a fiber tract can be compared. In previous work this has been accomplished primarily through voxel based tests that require sophisticated smoothing and multiple comparison correction. While this type of analysis is effective for hypothesis generation, the results are often challenging to interpret, and extremely strong differences are necessary to overcome multiple comparison correction. We propose to use a semi-parametric b-spline model of multivariate statistics along specific fiber bundles of interest as the basis

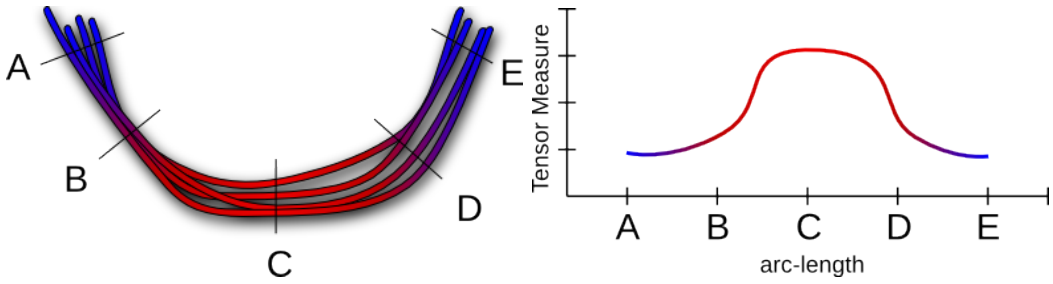

(a) Fiber bundle (b) Arc length Function

Fig. 4. The diffusion properties within a fiber bundle (a) are summarized as a function of arc length (b). For example, the FA value along the cross-section at points A,B,C,D,E are averaged and become the value of the function at the points A,B,C,D,E along the x-axis of the arc length function.

for group analysis.

3.1 Modeling of fiber tract properties

The diffusion properties of fiber tracts are modeled as smooth functions of arc length. In this model we reduce the diffusion data in a fiber bundle to a function of arc length for each tensor measure of interest. As illustrated in Fig. 4, tensor measures in a bundle are averaged at each cross-section along the bundle and to produce a function of arc length. In our framework template fiber bundles are computed in the tensor atlas using tractography, and the improved signal-to-noise ratio of the atlas allows reliable extraction of fiber bundles. The template fiber is warped back into the individual subject images to collect the diffusion data as shown in Fig. 1. Figure 6 shows an example of the template genu and splenium fiber bundles from a study and the individual functions produced for this bundle. Because the geometry of the individual fiber bundles are the same in atlas space, the data from each subject is parametrized consistently.

We have chosen to focus our analysis of diffusion properties on measures of tensor shape for two primary reasons. First, tensor orientation is an unstable measurement due to approximations of tensor reorientation during deformation. More importantly, however, invariant measures such as anisotropy and size can be linked more easily to changes in tissue properties. The most commonly used measurements of tensor shape are FA and MD to measure anisotropy and size respectively. However, it has been shown by Ennis and Kindlmann (2006) that FA and MD are not orthogonal. The non-orthogonality implies that differences in FA have different meanings depending on the magnitude of the MD. In this framework we have chosen to use FA because of its common usage in the literature. As a measure orthogonal to FA, the Frobenius norm of the tensor $\mathbf{D}$ is used as a measure of tensor size and is defined as

$$\|\mathbf{D}\| = \sqrt{\sum_{i=1}^{3}\sum_{j=1}^{3} D_{ij}^2} = \sqrt{\lambda_1^2 + \lambda_2^2 + \lambda_3^2}. \quad (1)$$

The mean diffusivity of the tensor, by comparison, is given by the sum of the eigenvalues rather than the sum of squared eigenvalues.

3.2 Statistics of tract models

The population of multivariate functions produced by the fiber tract model requires a new method for statistical inference. Image sampling as well as the fiber tract extraction process create a sampled representation of the fiber bundle diffusion properties. However, there exists a continuous underlying biology which generates these samples. Therefore, statistical analysis of the sampled diffusion functions must account for the underlying continuity and spatial correlation of the samples. We compute statistics of the diffusion curves as an infinite dimensional extension to multivariate statistics known as functional

data analysis (Ramsay and Silverman, 2005). The simplest extensions of ordinary statistics to the functional setting is the sample mean function $\bar{f}(t)$ given by

$$\bar{f}(t) = \frac{1}{N} \sum_{i=1}^{N} f_i(t), \tag{2}$$

and the sample variance-covariance function, which is the bivariate function,

$$v(s,t) = \frac{1}{N-1} \sum_{i=1}^{N} (f_i(s) - \bar{f}_i(s))(f_i(t) - \bar{f}_i(t)). \tag{3}$$

The diagonal of the function, $v(t,t)$, is the pointwise variance of the population of functions. Hypothesis testing and discriminant analysis of the space of functions has an inherent high-dimension, low-sample-size problem because of the infinite-dimensional space of continuous functions. Regularization methods are, therefore, essential in the computation of functional statistics. To enforce regularity, B-spline fitting and functional principal components analysis (PCA) is used for data-driven smoothing, where the number of retained PCA modes acts as a smoothing parameter.

In order to make computations tractable, smooth basis functions are fit to the sampled diffusion curves. B-splines were selected as basis functions due to the nonperiodic nature of the data, the compact support of the B-spline basis, and the ability to enforce derivative continuity. A large number of B-spline bases are first fit to the sampled functions using a least squares approach. The number of basis functions is chosen empirically to maintain local features while providing some smoothing. Computation of the mean function is computed by the sample mean of the B-spline coefficients. Computation of the variance-covariance function is more complex and requires accounting for the mapping between basis coefficients and function values. Let $f_i(t)$ be the B-spline function fit to the samples from subject i. Following the notation of

Ramsay and Silverman (2005), in matrix notation, we express all functions $f_i(t)$ as a matrix of coefficients $\mathbf{C}$ times the basis functions $\boldsymbol{\phi}$, so that

$$\mathbf{f}(t) = \mathbf{C}\boldsymbol{\phi}(t). \tag{4}$$

Assuming the functions have been centered about the sample mean, the variance-covariance function of $\mathbf{f}(t)$ can be written as

$$v(s,t) = \frac{1}{N-1}\boldsymbol{\phi}(s)^T\mathbf{C}^T\mathbf{C}\boldsymbol{\phi}(t). \tag{5}$$

PCA of the functions $f_i(t)$ decomposes $v(s,t)$ into the orthogonal unit eigenfunctions $\xi(t)$ which satisfy

$$\int v(s,t)\xi(t)dt = \lambda\,\xi(s). \tag{6}$$

Equation (6) can be solved numerically by rewriting in terms of the basis functions $\boldsymbol{\phi}$ as

$$\boldsymbol{\phi}(s)^T\mathbf{C}^T\mathbf{C}\boldsymbol{\phi}(t)\boldsymbol{\phi}(t)^T\mathbf{b} = \lambda\boldsymbol{\phi}(s)^T\mathbf{b} \tag{7}$$

Defining $\mathbf{W}$ is the matrix of basis function inner products with entries

$$W_{ij} = \int \phi_i(t)\phi_j(t), \tag{8}$$

Equation (7) can be simplified in the matrix form,

$$\frac{1}{N-1}\mathbf{C}^T\mathbf{C}\mathbf{W}\mathbf{b} = \lambda\mathbf{b}. \tag{9}$$

The B-Spline basis is not orthonormal resulting in a non-symmetric eigenvalue problem to solve (9). This minimization can be solved by the symmetric eigenvalue problem for the basis coefficients $\mathbf{b}$, with the change of variable $\mathbf{W}^{1/2}\mathbf{u} = \mathbf{b}$:

$$\frac{1}{N-1}\mathbf{W}^{1/2}\mathbf{C}^\mathbf{T}\mathbf{C}\mathbf{W}^{1/2}\mathbf{u} = \lambda\mathbf{u}. \tag{10}$$

In our analysis we consider a joint analysis of FA and Frobenius norm functions with basis coefficients $\mathbf{C}_1$ and $\mathbf{C}_2$ respectively. We therefore compute PCA from the eigenanalysis of $\mathbf{\Sigma}$, where

$$\begin{aligned} \mathbf{\Sigma}_{ij} &= \mathbf{W}^{1/2}\mathbf{C}_i^T\mathbf{C}_j\mathbf{W}^{1/2}, \text{ and} \\ \mathbf{\Sigma} &= \begin{bmatrix} \mathbf{\Sigma}_{11} & \mathbf{\Sigma}_{12} \\ \\ \mathbf{\Sigma}_{21} & \mathbf{\Sigma}_{22} \end{bmatrix}. \end{aligned} \tag{11}$$

Hypothesis testing and discriminant analysis is performed on the projection of the data onto the first K PCA modes, where K serves as a smoothing parameter. An example of the PCA modes for Genu tracts from one and two year old subjects is shown in Fig. 5. In this work, K is chosen to maintain 90% of the variability of the variance-covariance matrix. Let $\mathbf{x}_i$ and $\mathbf{y}_i$ be the projection of the curves from two population of functions onto the PCA space. In this space the basis mapping has already been incorporated and standard multivariate analysis can be applied. The normal parametric hypothesis test for mean differences is the Hotelling T^2 statistic,

$$T^2 = \frac{n_x n_y}{n_x + n_y}(\bar{\mathbf{x}} - \bar{\mathbf{y}})\mathbf{S}^{-1}(\bar{\mathbf{x}} - \bar{\mathbf{y}})^T \tag{12}$$

where $\mathbf{S}$ is the pooled covariance matrix. In order to relax the normality assumptions associated with the parametric test, we apply a permutation test based on the T^2 statistic to compute p-values (Nichols and Holmes, 2002).

The T^2 statistic is proportional to the difference between group means projected onto the subspace given by the Fisher linear discriminant (FLD),

$$\boldsymbol{\omega} = \mathbf{S}^{-1}(\bar{\mathbf{x}} - \bar{\mathbf{y}})^T. \tag{13}$$

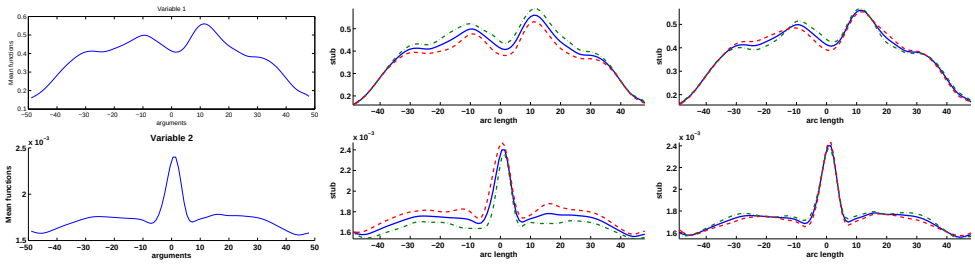

(a) Mean Functions (b) PCA 1 (c) PCA 2

Fig. 5. Visualization of the PCA modes for the joint analysis of FA and Frobenius norm are shown on the top and bottom rows respectively. The (a) mean functions for the combined population are shown with (b) the first and (c) second PCA modes. The first PCA mode accounts for a large percentage of the variability and shows constant changes FA with a corresponding anti-correlated change in Frobenius norm.

The linear discriminant, therefore, provides a direction for interpreting the detected group differences of the hypothesis test. The coefficients of the discriminant can be expanded into the original function basis so that $FLD(t) = \boldsymbol{\phi}(t)\boldsymbol{\omega}$ is a function whose inner product with the original data provides maximal separation between the groups. This function, $FLD(t)$, describes the localized changes of tensor parameters between the two groups.

4 Experiments

The registration framework of Section 2 along with the analysis method of Section 3 was applied to a clinical study of neurodevelopment. We have evaluated the effect of normal development on fiber tract properties from age one to two in cross-sectional populations. We have also performed hypothesis tests for differences between neonate control subjects and neonates with isolated mild ventriculomegaly (MVM).

4.1 Normal Development in Cross-Section from One to Two Years

The proposed methodology was evaluated on a cross-sectional study of normal development including subjects at one and two years of age. This was chosen as a test case because of the expected large differences in diffusion properties due to normal development. In this case the p-value of the hypothesis testing framework of Section 3 is less relevant as large changes are expected, but the discriminant direction provides localized information about the change in diffusion properties across age.

Subjects were imaged on a Siemens 3T Allegra scanner using a DTI protocol with 10 repetitions of a baseline image plus 6 diffusion weighted gradient directions using a b-value of $1000 s/mm^2$ and a voxel size of $2x2x2mm^3$. After image acquisition each repetition of the sequence were corrected for head motion by registration of the baseline images. The atlas building procedure of Section 2 was applied to a database of 49 healthy controls including 22 one year old subjects and 27 two year old subjects. The transformations were initialized to a template T2 atlas specific built from a set of two year old images. The feature image for atlas building was computed with a Gaussian kernel width of $\sigma = 2.0mm$, and atlas building was performed in a multi-resolution framework.

After registration and averaging, the atlas tensor image was used to identify four tracts of interest: genu, splenium, left cortico-spinal tract, and right cortico-spinal tract. A standard tractography algorithm using Runge-Kutta integration of the principal eigenvector field was used to extract the fiber tracts. Fibers were tracked from manually drawn seed regions in the atlas image and

constrained to pass through a manually drawn target region. For tractography in the atlas image a minimum FA threshold of 0.08 was used. As mentioned in Section 2, the atlas image provides improved SNR which allows lower FA thresholds than typically used for processing of single images. The atlas image and the four template tracts are shown in Fig. 10.

After generation of the atlas template tracts, data from the individual subject images was mapped on to these tracts using the transformations created during atlas building. Tract oriented functions were then computed for each subject using an origin defined in the atlas. Thirty b-spline control points were used to fit each function, and the resulting functions for the genu, splenium, and the left and right cortico-spinal tracts are shown in Figs. 6 and 7. After evaluation of the variance-covariance matrix for each tract, the number of PCA modes for the tract was selected to maintain 90% of the variance resulting in between 6-10 PCA modes per tract. Permutation testing over the Hotelling T^2 statistics was run for each tract, and the FLD associated with the null permutation was computed for visualization. The resulting p-values as well as the maximum and average pointwise differences of diffusion measures between groups along the tract are summarized in Table 1. All the tracts indicate a general trend of increase in FA and a correlated decrease in Frobenius norm from one to two year old groups. Figure 8 shows a visualization of the discriminant function for the genu tract that indicates an increase in FA and a correlated decrease in Frobenius norm from the one year to two year old groups with the effect focused in the center of the tract and trailing off as the tract enters the grey matter regions of the cortex. In the cortico-spinal tracts there is some evidence of localized changes. Figure 9 shows the mean functions for the two groups and the discriminant direction. The discriminant indicates that FA increases from

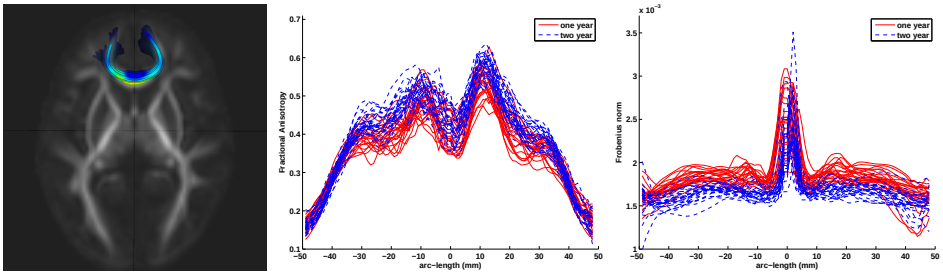

(a) Genu (b) FA curves (c) Norm curves

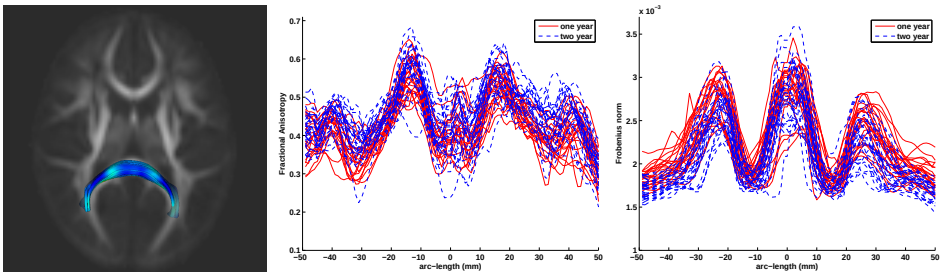

(d) Splenium (e) FA curves (f) Norm curves

Fig. 6. (a) Genu and (d) splenium tracts extracted from the tensor atlas with color indicating mean FA value. The diffusion values are sampled along the atlas-normalized arc length for each individual in the study for FA and Frobenius norm values. The sampled FA and Frobenius norm functions for the two groups are shown in (b), (c), (e), (f). The one year old subjects are the dashed red lines and the two year old subjects are the solid blue lines. The spikes in the center of the Frobenius norm functions for the genu are likely due to partial voluming with the fluid spaces.

one to two years in regions of the tract inferior of the callosal fibers, while the FA decreases in regions at the callosal fibers and above. This localized change could indicate a possible increase in orientation complexity or crossing fibers during development.

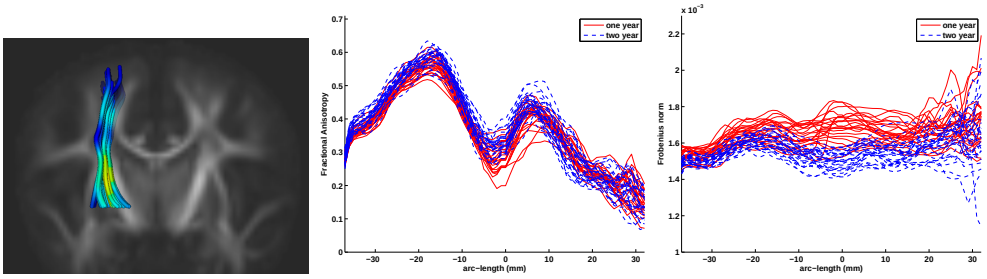

(a) Left cortico-spinal (b) FA curves (c) Norm curves

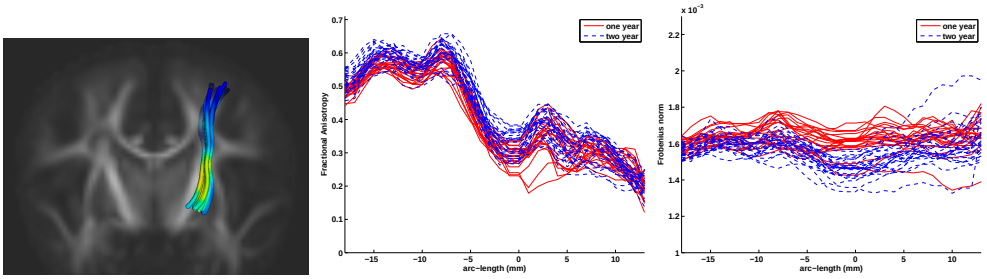

(d) Right cortico-spinal (e) FA curves (f) Norm curves

Fig. 7. (a) Left and (d) right cortico-spinal tracts in the one and two year old population. The tracts are sampled from inferior to superior along the tract to produce the sampled functions in (b),(c), (e), and (f).

4.2 Hypothesis Testing Between Controls and MVMs in Neonate Imaging

Prenatal MVM is a condition characterized by enlargement of the lateral ventricles diagnosed by ultrasound and has been associated with increased risk of neuropsychatric disorders (Gilmore et al., 1998). Previous investigation of DTI quantities in MVM have found significant a decrease in FA from controls in manually identified regions of splenium as well as significant increase in MD in regions of the genu, splenium, and cortico-spinal tracts (Gilmore et al., 2007b).

The atlas building method described in Section 2 was applied to a database of 114 images including 85 controls, 13 MVMs, 12 offsprings of schizophrenics, and 4 offsprings of bi-polar. Transformations were initialized to a neonate

Table 1

Tract differences from one to two years

Tract	p-value	FA		Frobenius norm	
		max	avg	max	avg
Genu	**<.0001**	.067	.025	-4.0×10^{-4}	-1.6×10^{-4}
Splenium	**.0024**	.053	.022	-2.6×10^{-4}	-1.4×10^{-4}
Left cortico-spinal	**.0004**	.036	.014	-1.9×10^{-4}	-0.9×10^{-4}
Right cortico-spinal	**.0002**	.049	.023	-1.3×10^{-4}	-0.7×10^{-4}

The table provides p-values for the hypothesis test of differences between one and two year old subjects. Columns 3-4 and 5-6 show the maximum and average point-wise differences between the mean functions of the two groups.

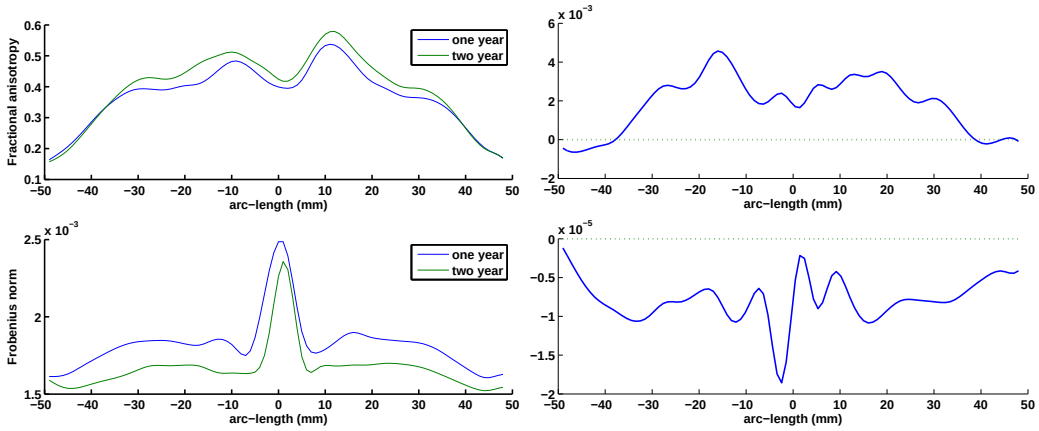

(a) Genu mean functions (b) Genu discriminant functions

Fig. 8. (a) The mean functions for the genu tract one and two year old groups along with (b) the linear discriminant which describes the function that maximizes separation between the groups. Here, the FA values increase from one to two years, and the Frobenius norm values decrease in a correlated manner. The FA changes are localized towards the center of the tract and are less informative at both the left and right ends of the tract.

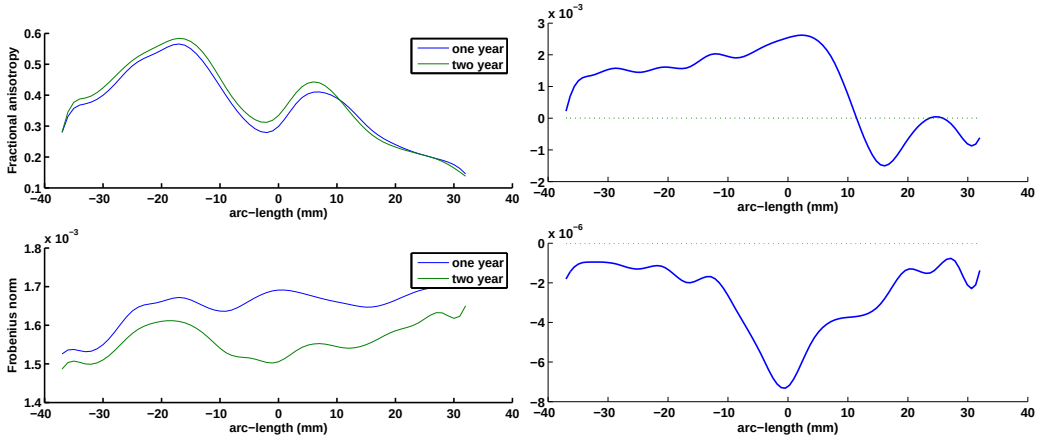

(a) Left cortico-spinal mean functions (b) Left cortico-spinal discriminant

Fig. 9. (a) The mean functions of the left cortico-spinal tract for the one and two year old groups along with (b) the linear discriminant which describes the function which maximizes separation between the groups. Here FA increases in regions inferior of the callosal fibers and decreases as the tract passes near the corpus callosum. This could indicate increased interaction and crossing between fibers in this region.

specific template with T2 weighting. The resulting images were upsampled by 20% to prevent data loss during the non-rigid registration. The feature image was computed at $\sigma = 1.5mm$ for each subject, and the atlas building procedure was applied in a multi-resolution framework using three levels. After diffeomorphic registration of each tensor image, an atlas tensor image was created by averaging the deformed images. In atlas tensor image, tracts were computed for the genu, splenium, and left and right cortico-spinal tract.

Analysis of tracts was performed on the left and right cortico-spinal tracts, genu, and splenium. Statistically significant differences were found in the splenium tract but not the genu or cortico-spinal tracts. Figure 11 shows the discriminant direction for the splenium tract and indicates a decrease in FA and a correlated increase in Frobenius norm from control subjects to those with MVM. Results for all analyzed tracts are summarized in Table 2.

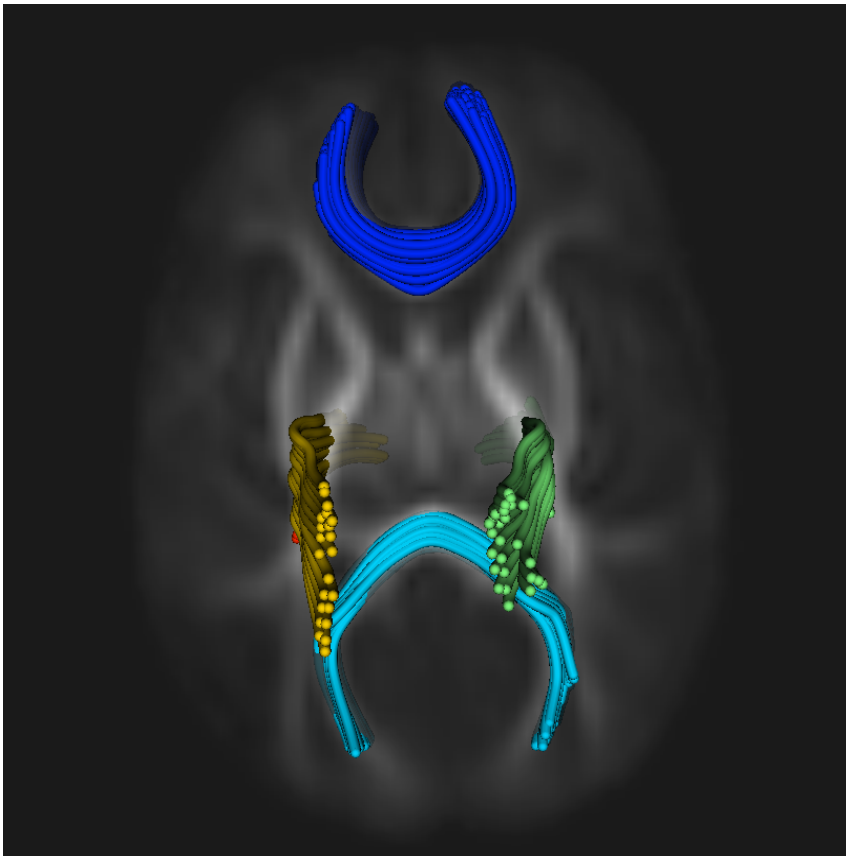

Fig. 10. Template fiber tracts in atlas of neonate subjects overlaid on the FA image of the atlas.

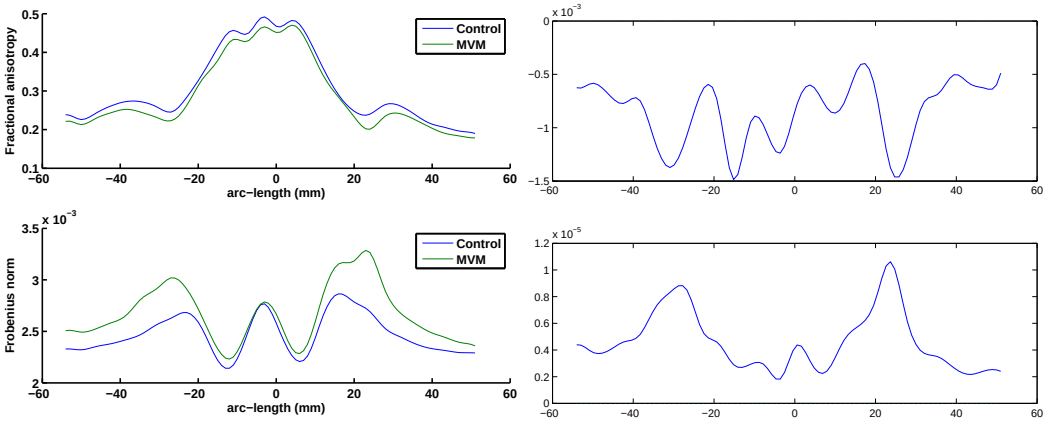

Fig. 11. (a) The mean functions for the splenium tract in control and MVM neonates are shown along with the (b) Fisher linear discriminant. The discriminant indicates that the significant differences in tract properties are attributed to an decrease in FA and a increase in Frobenius norm in MVMs.

Table 2

Tract differences from neonate controls to MVMs

Tract	p-value	FA		Frobenius norm	
		max	avg	max	avg
Genu	.99	.0086	.0020	1.1×10^{-4}	0.32×10^{-4}
Splenium	**.0001**	.039	-.019	5.7×10^{-4}	2.1×10^{-4}
Left cortico-spinal	.24	.016	.00015	1.5×10^{-4}	-0.6×10^{-4}
Right cortico-spinal	.80	.022	.0034	8.8×10^{-5}	-2.6×10^{-5}

The table provides p-values for the hypothesis test of differences between controls and MVMs. Columns 3-4 and 5-6 show the maximum and average pointwise differences between the mean functions of the two groups.

5 Conclusion and Discussion

We have presented a method for making inferences about group differences in fiber tract diffusion properties. Our framework combines a method for spatial normalization of tensor images with a method for quantitative tract analysis. Within this framework we apply a novel method for joint analysis of tensor shape parameters using statistical inference of populations of multivariate continuous functions. The statistical framework provides a method for both hypothesis testing and localizing the differences determined by the hypothesis test.

There are several limitations to the proposed methodology that should be noted. First, the atlas building methodology of Section 2 assumes that the overall appearance of DTI images is sufficiently similar between the two groups that registration to a single coordinate system is feasible, as is common in

brain mapping approaches. In studies where subjects with severe geometric distortions such as tumors are present, this approach is likely not feasible. Secondly, tracts which are small or inconsistent even among the same group will be challenging to identify in the atlas. For this reason, we have focused on large major fiber bundles, where consistency is expected. Finally, the statistical analysis relies on tensor shape measures to make inference about potential changes in tissue structure. However, there are several other effects which could have an impact on the tensor shape besides tissue change. For example, varying degrees of partial voluming effects can cause differences in total diffusivity that do not necessarily reflect changes in axon density or myelination (Peled, 2007). Further studies are necessary to investigate the underlying biological cause of detected differences in DTI measures.

In this work, we have focused on analysis of the diffusion tensor model rather than high angular resolution diffusion imaging (HARDI) models. This is done primarily because of the constraints of currently available clinical data. In the future we anticipate that some level of higher order modeling will be required to fully capture the geometry of anatomical fiber bundles and resolve fiber crossings. The statistical analysis presented in this paper can be readily extended to more complex information given appropriate measures of diffusion shape for more complex models. For example the generalized measures presented by Özarslan et al. (2005) could be used within the same framework. More advanced tractography methods incorporating HARDI data could also improve the generation of the template fiber tract.

In summary, we have presented a novel method for detecting and understanding differences between diffusion properties of DTI fiber bundles. The methodology is demonstrated on a clinical study of neurodevelopment. In this study

changes between one and two year populations were assessed and localized in several key tracts. Previous results from an ROI based study were confirmed in differences between neonate controls and MVMs.

Acknowledgements

This work is part of the National Alliance for Medical Image Computing (NA-MIC), funded by the National Institutes of Health through Grant U54 EB005149. Information on the National Centers for Biomedical Computing can be obtained from `http://nihroadmap.nih.gov/bioinformatics`. We also acknowledge support from the NIMH Silvio Conte Center for Neuroscience of Mental Disorders MH064065.

References

Alexander, D., Pierpaoli, C., Basser, P. J., Gee, J., Nov. 2001. Spatial transformations of diffusion tensor magnetic resonance images. Medical Imaging, IEEE Transactions on 20 (11), 1131–1140.

Arsigny, V., Fillard, P., Pennec, X., Ayache, N., 2006. Log-Euclidean metrics for fast and simple calculus on diffusion tensors. Magnetic Resonance in Medicine 56 (2), 411–421.

Barnea-Goraly, N., Kwon, H., Menon, V., Eliez, S., Lotspeich, L., Reissa, A. L., Feb. 2004. White matter structure in autism: preliminary evidence from diffusion tensor imaging. Biological Psychiatry 55 (3), 323–326.

Basser, P., Pierpaoli, C., Jun. 1996. Microstructural and physiological features

of tissues elucidated by quantitative DT-MRI. Journal Magnetic Resonance 111 (3), 209–219.

Basser, P. J., Pajevic, S., Pierpaoli, C., Duda, J., Aldroubi, A., 2000. In Vivo Fiber Tractography Using DT-MRI Data. Magnetic Resonance in Medicine 44 (4), 625–632.

Bonekamp, D., Nagae, L. M., Degaonkar, M., Matson, M., Abdalla, W. M., Barker, P. B., Mori, S., Horská, A., 2007. Diffusion tensor imaging in children and adolescents: Reproducibility, hemispheric, and age-related differences. NeuroImage 34, 733–742.

Burns, J., Job, D., Bastin, M. E., Whalley, H., Macgillivray, T., Johnstone, E. C., Lawrie, S. M., 2003. Structural disconnectivity in schizophrenia: a diffusion tensor magnetic resonance imaging study. The British Journal of Psychiatry 182 (5), 439–443.

Corouge, I., Fletcher, P. T., Joshi, S., Gouttard, S., Gerig, G., 2006. Fiber tract-oriented statistics for quantitative diffusion tensor MRI analysis. Medical Image Analysis 10 (5), 786–798.

Ennis, D. B., Kindlmann, G., Jan. 2006. Orthogonal tensor invariants and the analysis of diffusion tensor magnetic resonance images. Magnetic Resonance in Medicine 55 (1), 136–146.

Fletcher, P. T., Joshi, S., 2007. Riemannian Geometry for the Statistical Analysis of Diffusion Tensor Data. Signal Processing 87 (2), 250–262.

Fletcher, P. T., Tao, R., Joeng, W.-K., Whitaker, R., 2007. A Volumetric Approach to Quantifying Region-to-Region White Matter Connectivity in Diffusion Tensor MRI. In: Information Processing in Medical Imaging. Vol. 4584 of LNCS. pp. 346–358.

Gilmore, J. H., Lin, W., Corouge, I., Vetsa, Y. S., Smith, J. K., Kang, C., Gu, H., Hamer, R. A., Lieberman, J. A., Gerig, G., Nov. 2007a. Early Post-

natal Development of Corpus Callosum and Corticospinal White Matter Assessed with Quantitative Tractography. American Journal of Neuroradiology 28 (9), 1789–1795.

Gilmore, J. H., Smith, L., Kang, C., Hamer, R., Wolfe, H., Hertzberg, B., Smith, J. K., Chescheir, N., Lin, W., Gerig, G., Dec. 2007b. Neonatal Brain Structure in Children with Prenatal Isolated Mild Ventriculomegaly. In: Proceedings ACNP 2007 American College of Neuropsychopharmacology, 46th annual meeting. Boca Raton, FL.

Gilmore, J. H., van Tol, J., Kliewer, M. A., Silva, S. G., Cohen, S. B., Hertzberg, B. S., Chescheir, N. C., Oct. 1998. Mild ventriculomegaly detected in utero with ultrasound: clinical associations and implications for schizophrenia. Schizophrenia Research 33 (3), 133–140.

Goodlett, C., Davis, B., Jean, R., Gilmore, J., Gerig, G., 2006. Improved Correspondance for DTI population studies via unbiased atlas building. In: Medical Image Computing and Computer Assisted Intervention (MICCAI). Vol. 4191 of LNCS. Springer-Verlag, pp. 260–267.

Guo, A. C., Petrella, J. R., Kurtzberg, J., Provenzale, J. M., 2001. Evaluation of White Matter Anisotropy in Krabbe Disease with Diffusion Tensor MR Imaging: Initial Experience. Radiology 218 (3), 809–815.

Hermoye, L., Saint-Martin, C., Cosnard, G., Lee, S.-K., Kim, J., Nassogne, M.-C., Menten, R., Clapuyt, P., Donohue, P. K., Hua, K., Wakana, S., Jiang, H., van Zijl, P. C., Mori, S., 2006. Pediatric diffusion tensor imaging: Normal database and observation of the white matter maturation in early childhood. NeuroImage 29 (2), 493–504.

Jones, D., Griffin, L., Alexander, D., Catani, M., Horsfield, M., Howard, R., Williams, S., 2002. Spatial normalization and averaging of diffusion tensor MRI data sets. Neuroimage 17 (2), 592–617.

Jones, D. K., Symms, M. R., Cercignani, M., Howard, R. J., Jun. 2005a. The effect of filter size on VBM analyses of DT-MRI data. NeuroImage 26 (2), 546–554.

Jones, D. K., Travis, A. R., Eden, G., Pierpaoli, C., Basser, P. J., 2005b. PASTA: pointwise assessment of streamline tractography attributes. Magnetic Resonance in Medicine 53 (6), 1462–1467.

Joshi, S., Davis, B., Jomier, M., Gerig, G., Nov. 2004. Unbiased diffeomorphic atlas construction for computational anatomy. NeuroImage 23 (Supplement1), S151–S160.

Kindlmann, G., Tricoche, X., Westin, C.-F., 2007. Delineating white matter structure in diffusion tensor MRI with anisotropy creases. Medical Image Analysis 11 (5), 492–502.

Kubicki, M., Park, H., Westin, C., Nestor, P., Mulkern, R., Maier, S., Niznikiewicz, M., Connor, E., Levitt, J., Frumin, M., Kikinis, R., Jolesz, F., McCarley, R., Shenton, M., Jul. 2005. DTI and MTR abnormalities in schizophrenia: Analysis of white matter integrity. NeuroImage 26 (3), 1109–1118.

Lin, F., Yu, C., Jiang, T., Li, K., Li, X., Qin, W., Sun, H., Chan, P., Oct. 2006. Quantitative analysis along the pyramidal tract by length-normalized parameterization based on diffusion tensor tractography: Application to patients with relapsing neuromyelitis optica. Neuroimage 33 (1), 154–160.

Melonakos, J., Mohan, V., Niethammer, M., Smith, K., Kubicki, M., Tannenbaum, A., 2007. Finsler Tractography for White Matter Connectivity of the Cingulum Bundle. In: Medical Image Computing and Computer Assisted Intervention (MICCAI). Vol. 4791 of LNCS. Springer-Verlag, pp. 36–43.

Mori, S., Wakana, S., Nagae-Poetscher, L. M., Van Zijl, P. C., 2005. MRI Atlas of Human White Matter, 1st Edition. Elsevier.

Nichols, T. E., Holmes, A. P., 2002. Nonparametric Analysis of functional neuroimaging: A Primer with Examples. Human Brain Mapping 15 (1), 1–25.

O'Donnell, L., Westin, C.-F., Nov. 2007. Automatic Tractography Segmentation Using a High-Dimensional White Matter Atlas. Medical Imaging, IEEE Transactions on 26 (11), 1562–1575.

Özarslan, E., Vemuri, B. C., Mareci, T. H., 2005. Generalized Scalar Measures for Diffusion MRI Using Trace, Variance, and Entropy. Magnetic Resonance in Medicine 53, 866 – 876.

Peled, S., 2007. New Perspectives on the Sources of White Matter DTI Signal. Medical Imaging, IEEE Transactions on 26 (11), 1448–1455.

Pennec, X., Fillard, P., Ayache, N., January 2006. A Riemannian framework for tensor computing. International Journal of Computer Vision 66 (1), 41–66.

Peyrat, J.-M., Sermesant, M., Pennec, X., Delingette, H., Chenyang Xu, McVeigh, E., Ayache, N., Nov. 2007. A Computational Framework for the Statistical Analysis of Cardiac Diffusion Tensors: Application to a Small Database of Canine Hearts. Medical Imaging, IEEE Transactions on 26 (11), 1500–1514.

Ramsay, J., Silverman, B., 2005. Functional Data Analysis, 2nd Edition. Springer.

Salvador, R., Peña, A., Menon, D. K., Carpenter, T. A., Pickard, J. D., Bullmore, E. T., Feb. 2005. Formal characterization and extension of the linearized diffusion tensor model. Human Brain Mapping 24 (2), 144–155.

Smith, S. M., Jenkinson, M., Johansen-Berg, H., Rueckert, D., Nichols, T. E., Mackay, C. E., Watkins, K. E., Ciccarelli, O., Cader, M. Z., Matthews, P. M., Behrens, T. E., 2006. Tract-based spatial statistics: Voxelwise analysis of

multi-subject diffusion data. NeuroImage 31, 1487–1505.

Snook, L., Plewes, C., Beaulieu, C., 1 Jan. 2007. Voxel based versus region of interest analysis in diffusion tensor imaging of neurodevelopment. NeuroImage 34 (1), 243–252.

Sydykova, D., Stahl, R., Dietrich, O., Ewers, M., Reiser, M. F., Schoenberg, S. O., Möller, H.-J., Hampel, H., Teipel, S. J., 2007. Alzheimer's Disease: A Diffusion Tensor Imaging and Voxel-Based Morphometry Study. Cerebral Cortex 17 (10), 2276–2282, in Press.

Xu, D., Hao, X., Bansal, R., Plessen, K. J., Peterson, B. S., Mar. 2008. Seamless warping of diffusion tensor fields. Medical Imaging, IEEE Transactions on 27 (3), 285–299.

Xu, D., Mori, S., Shen, D., van Zijl, P. C., Davatzikos, C., Jul. 2003. Spatial normalization of diffusion tensor fields. Magnetic Resonance in Medicine 50 (1), 175–182.

Yushkevich, P. A., Zhang, H., Simon, T. J., Gee, J. C., Jun. 2008. Structure-specific statistical mapping of white matter tracts. NeuroImage 41 (2), 448–461.

Zhang, H., Avants, B. B., Yushkevich, P. A., Woo, J. H., Wang, S., McCluskey, L. F., Elman, L. B., Melhem, E. R., Gee, J. C., Nov. 2007. High-dimensional spatial normalization of diffusion tensor images improves the detection of white matter differences in amyotrophic lateral sclerosis. Medical Imaging, IEEE Transactions on - Special Issue on Computational Diffusion MRI 26 (11), 1585–1597.